LAWRENCE
LIVERMORE
NATIONAL
LABORATORY

LLNL-JRNL-579942

# Coexistence of the Alpha and Delta Phases in As-Cast Uranium-Rich U-Zr Alloys

J. T. McKeown, S. Irukuvarghula, S. Ahn, M. Wall, L. L. Hsiung, S. McDeavitt, P. E. A. Turchi

September 10, 2012

Journal of Nuclear Materials

## Disclaimer

**Coexistence of the α and δ phases in an as-cast uranium-rich U-Zr alloy**

J.T. McKeown[a,*], S. Irukuvarghula[b], S. Ahn[b], M. Wall[a], L.L. Hsiung[a], S. McDeavitt[b], and P.E.A. Turchi[a]

[a] Condensed Matter and Materials Division, Lawrence Livermore National Laboratory, Livermore, CA 94550, USA

[b] Department of Nuclear Engineering, Texas A&M University, College Station, TX 77843, USA

**Abstract**

Uranium-zirconium alloys are being investigated for use in ultrahigh burn-up, metallic inert matrix nuclear fuels. Characterization of these alloys in the transmission electron microscope with spatial resolutions that are inaccessible by other techniques shows that the orthorhombic αand hexagonalδ phases coexist in an as-cast uranium-rich U-10wt.%Zr alloy. Analyses reveal the chemistries of and crystallographic relationship between the two phases.

*Keywords:* Metal and alloys; uranium; microstructure; transmission electron microscopy

* Corresponding author. *Tel.*: 1-925-422-1708. *Email*: mckeown3@llnl.gov.

Inert matrix fuels (IMF) [1-4] are advanced nuclear fuel forms that can provide higher burn-up than current fuel forms, making them a promising alternative for future-generation nuclear power reactors. One of the alloy systems being considered as metallic fuel in the IMF design is U-Zr. Uranium-rich U-Zr alloys provide a combination of excellent properties that make them strong candidate alloys for metallic actinide fuels: a low thermal neutron cross-section, improved corrosion resistance, and enhanced dimensional stability under irradiation and thermal cycling at elevated temperatures [5]. Of key importance to the development of metallic actinide fuel materials for IMF designs is an understanding of the thermodynamics and kinetics of fuel phase stability and evolution under both thermal and irradiation conditions through structural characterization.

The U-Zr equilibrium phase diagram [6-9] shows that at temperatures below ~610°C, uranium-rich U-Zr alloys consist of a two-phase structure of orthorhombic α-uranium with limited zirconium solubility and the hexagonal, zirconium-rich intermetallic δ phase ($UZr_2$). Early studies of as-cast uranium-rich U-Zr alloys [10-12] indicated the coexistence of the two equilibrium phases at room temperature, but no experimental evidence was provided. A two-phase precipitate structure consisting of small globules and rods in as-cast U-Zr alloys of 5, 10, and 20wt.%Zr was reported [10]. There has been no experimental evidence provided for the coexistence of the α and δ phases in as-cast uranium-rich U-Zr alloys, despite numerous studies using a variety of techniques [13-18], including X-ray diffraction (XRD) analysis, optical microscopy, scanning electron microscopy (SEM), and dilatometry. The absence of the δ phase has been attributed to sluggish kinetics due to low interdiffusivity in U-Zr solid solutions

[19,20], resulting in only Zr-supersaturated α phase at room temperature in as-cast alloys from 2–10wt.%Zr [14-18]. The presence of the δ phase in uranium-rich U-Zr alloys has only been observed after prolonged anneals (hundreds to thousands of hours) at elevated temperatures [17,18], and it has been concluded that the formation of δ phase in as-cast uranium-rich U-Zr alloys is highly unlikely [17].

The present study was focused on assessment of the thermal stability of as-cast uranium-rich U-Zr alloys prior to irradiation studies, in order to distinguish between the two effects when considering their potential use as metallic fuel in the IMF design. Structural characterization was conducted using the high spatial resolution of the transmission electron microscope (TEM), and it will be shown that the α and δ phases coexist in a fine-scale structure in the observed as-cast uranium-rich U-Zr alloy.

A uranium-rich U-Zr alloy of 10wt.%Zr (U-10Zr) was produced using crystal bar zirconium and pieces of depleted uranium that were washed in nitric acid to remove the surface oxide layer. The alloy was melt-cast in an yttria crucible under argon atmosphere in a high-temperature furnace. The sample was heated at a rate of 50°/min from room temperature to ~1900°C, where it was held isothermally for 1 h before cooling to room temperature at a rate of 30°C/min. The alloy slug was then flipped and melted again under the same conditions to ensure homogeneity. The final size of the cylindrical as-cast alloy was ~3 cm in length and 1.25 cm in diameter. The alloy was then sectioned and polished to a 0.05-μm finish for XRD analysis. XRD experiments were conducted with an APD 3720 Philips XRD vertical goniometer using $CuK_{\alpha}$ radiation. TEM specimens were prepared by mechanical thinning to a thickness of ~200 μm, followed by electropolishing using a 10% perchloric acid/90% acetic acid solution at 15°C and a

voltage of 40 V. Conventional $Ar^+$ ion milling was used to further thin the specimens if necessary. Samples were transferred directly to the TEM after electropolishing or ion milling, but a thin oxide layer will form on the TEM sample during this transfer. Samples were stored in a vacuum desiccator when not in the TEM and briefly ion milled again to remove surface oxide prior to reinsertion into the TEM. TEM analysis was conducted on a Philips CM300 FEG ST TEM operating at an accelerating voltage of 300 kV. The TEM is equipped with a Gatan Imaging Filter (GIF) and a detector for energy dispersive spectrometry (EDS). EDS analysis was conducted using a 12 nm electron probe.

Figure 1 shows the experimental XRD pattern obtained from the U-10Zr alloy. Inspection of the XRD data indicates that the alloy consists of the $\alpha$ phase only, as all of the diffraction peaks correspond to $\alpha$-U with the exception of a few weak peaks that are the result of surface oxide on the polished alloy sample (the positions and relative intensities of the diffraction peaks for $\alpha$-U, $UZr_2$, and $UO_2$ are provided in Fig. 1). Notably absent are peaks that correspond to the $\delta$-$UZr_2$ phase. These XRD results are consistent with those of previous studies involving U-10Zr alloys [13,14,17]. However, also consistent with prior studies [13,14,17], optical and SEM micrographs revealed a lamellar structure suggesting the presence of two phases. This lamellar structure was concluded to be the product of a monotectoid reaction ($\beta$ and $\gamma''$ transforming to $\alpha$), with the lamellae consisting only of supersaturated $\alpha$ phase [13,14,17]. TEM analysis was conducted to further assess the nature of this lamellar structure.

Bright-field images of the as-cast U-10Zr alloy are presented in Figure 2, showing the morphology of the lamellar structure. The lamellae have an average peak-to-peak spacing of 73.9 ± 11.6 nm, as measured from line profiles across multiple bright-field

images [21]. Figure 2(b) shows that multiple variants of the lamellar structure are present in the alloy. Here, they are approximately orthogonal to one another, but multiple orientations between lamellar regions exist in the alloy. Determination of the orientations between these variants could potentially provide insight to the transformation mechanism from the high-temperature BCC $\gamma$ solid solution [6-9] to the observed lamellar structure.

Compositional analysis using EDS in the TEM revealed that the lamellar structure consists of the uranium-rich $\alpha$ phase and the zirconium-rich $\delta$ phase. Figure 3 shows representative spectra from both the $\alpha$ and $\delta$ phases (dark and light contrast, respectively, as labeled in the inset image). The average compositions of the $\alpha$ and $\delta$ phases, measured in 10 distinct lamellae of each phase, were 99 ($\pm$ 0.5) wt.%U, 1 ($\pm$ 0.5) wt.%Zr and 58 ($\pm$ 4) wt%U, 42 ($\pm$ 4) wt%Zr, respectively. Using the overall composition of the alloy (10wt.%Zr) and the lever rule, the weight fractions of the phases were calculated to be ~0.78 $\alpha$ and 0.22 $\delta$, which, when combined with the densities of the two phases ($\rho_\alpha$ = 19.05 g/cm$^3$; $\rho_\delta$ = 9.84 g/cm$^3$ [9]), gives volume fractions of 0.65 $\alpha$ and 0.35 $\delta$, well within experimental error of what the phase diagram predicts at room temperature (0.66 $\alpha$ and 0.34 $\delta$). This is also consistent with the lamellar widths of the two phases shown in the bright-field images of Figure 2. The EDS spectra in Figure 3 also display carbon and oxygen peaks. There may be small amounts of carbon and oxygen dissolved in the alloy, but the carbon peak is likely the result of hydrocarbons adsorbed to the surface of the specimen (introduced during sample preparation and contamination in the TEM) while the oxygen peak is likely due to a surface oxide on the TEM specimen, evident in diffraction patterns (see, for example, Fig. 4(b)).

The crystallography of the α and δ phases and crystallographic relations between the lamellae were investigated using selected-area electron diffraction. Figure 4 provides experimental diffraction patterns acquired from two variants of the lamellar structure, along with matching simulated diffraction patterns showing the orientation between the lamellae and the zone axes in which the patterns were recorded. The experimental diffraction patterns confirm that the phases present were the orthorhombic α and hexagonal δ phases (see Table 1 for crystallographic data of the two phase), and the orientation relationships between the two lamellar phases in Figure 4(a) and (b) were:

$$\text{(a): } (010)[100]_{\alpha}||(0\bar{1}10)[0001]_{\delta}$$

$$\text{(b): } (010)[001]_{\alpha}||(0\bar{1}10)[2\bar{1}\bar{1}0]_{\delta}$$

These observed orientation relationships are the same, rotated 90° from one another about the [020] direction of the α phase ($[0\bar{1}10]$ direction of the δ phase). The orientation relationship also reveals that the interface plane between the two lamellar phases consists of the $(010)_{\alpha}$ plane of the α phase and the prismatic $(0\bar{1}10)_{\delta}$ plane (*m*-plane) of the δ phase. It should be noted that within a single variant of the lamellar structure, all of the alternating lamellae of each respective phase are of the same orientation, with no indication of rotation, inversion, or twinning.

While the electron diffraction data verify that the α and δ phases coexist with a distinct crystallographic relationship and the measured compositions are reasonable based on the equilibrium phase diagram and previous assessments of homogeneity ranges [7-9,20,22], the Zr content in the δ phase at room temperature was lower than what the phase diagram predicts and higher in α-U than the maximum solubility even at temperatures of 500°C (0.09 wt.%) [23], indicating that the structure has not reached

equilibrium. The curved nature of the interfaces between the two phases, evident in Figure 2, provides further evidence of a non-equilibrium structure, as these interfaces would likely sharpen and straighten with increased time at temperature. However, based on the observations presented, the formation of the δ phase in uranium-rich U-Zr alloys may not be as kinetically sluggish as previously suggested [14-18].

Finally, what accounts for the discrepancies between TEM observations and analyses and those of other characterization techniques that have been unable to detect the δ phase in as-cast, uranium-rich U-Zr alloys? As mentioned above, the XRD results in Figure 1 are consistent with those of previous studies [13,14,17] and indicate that the alloy consists of α-U only, even though the volume fraction of δ phase should be within the detection limits of XRD techniques. But within the 2Θ angular range spanned during XRD experiments, almost all reflections that correspond to the δ phase overlap with either the α-U phase or oxide. Upon closer inspection of the experimental XRD data in Figure 1, there appears to be a weak peak at ~72°, which could correspond to the δ phase, but this cannot be stated conclusively. Another concern is the high linear absorption coefficients of uranium and uranium-rich alloys for X-rays with energies employed in XRD experiments. Using the TEM EDS measurements for the compositions and weight fractions of the α and δ phases with the mass absorption coefficients of U and Zr [24] for $CuK_\alpha$ X-rays yields a weighted mass absorption coefficient of 290.1 $cm^2/g$ for the specimen. The average density of the sample was 17.02 $g/cm^3$ based on the densities of the two phases and the measured weight fractions. Thus, 99% of the incident X-ray intensity would be absorbed in a surface layer that is only ~9 μm thick. Combined with the lower volume fraction and small size of the δ-phase lamellae, detection of those peaks

with little overlap is likely hindered by a combination of low intensity and experimental broadening effects. This could also help explain detection of the δ phase in XRD patterns after long anneals [17,18], as the lamellar structure would coarsen over extended heat treatments, potentially alleviating some of these issues.

While optical and SEM micrographs suggested the presence of a two-phase structure, compositional analysis using EDS in the SEM is complicated by the large excitation volume of the electron probe in the specimen relative to the size of the lamellae. EDS chemical analysis of the same U-10Zr sample in the SEM measured a composition of ~4wt.%Zr, consistent with previous results [13,14,17] that suggest a supersaturated α phase. However, both the penetration depth and width of, for example, 20 keV electrons in a U-10wt.%Zr alloy are ~0.5 μm based on calculations using empirical [25] and theoretical [26] expressions available in the literature. Clearly, the excitation volume spans multiple lamellae, leading to measurement of an "average" composition dependent on volume fraction. In contrast, thin foils and small electron probes in the TEM minimize these issues, allowing characterization of individual lamellae with high spatial resolution.

In summary, we have provided experimental evidence for the coexistence of the α and δ phases in an as-cast uranium-rich U-Zr alloy. Imaging, diffraction, and compositional analysis in the TEM all self-consistently reveal the fine-scale lamellar structure to be alternating α and δ phases with a specific crystallographic relationship. TEM analysis is therefore crucial to properly characterize these nuclear fuels, particularly with fine-scale structures that require high spatial resolutions for accurate analyses.

This work was performed under the auspices of the U.S. Department of Energy by Lawrence Livermore National Laboratory under Contract DE-AC52-07NA2734. Work was funded by the Laboratory Directed Research and Development Program at LLNL under project tracking code 12-SI-008.

## References


[1] A.M. Savchenko, A.V. Vatulin, A.V. Morozov, I.V. Dobrikova, S.A. Ershov, S.V. Maranchak, Z.N. Petrova, Y.V. Konovalov, J. Nucl. Mater., 352 (2006) 334.

[2] A.M. Savchenko, A.V. Vatulin, A.V. Morozov, V.L. Sirotin, I.V. Dobrikova, G.V. Kulakov, S.A. Ershov, V.P. Kostomarov, Y.I. Stelyuk, J. Nucl. Mater., 352 (2006) 372.

[3] A. Savchenko, I. Konovalov, A. Vatulin, A. Morozov, V. Orlov, O. Uferov, S. Ershov, A. Laushkin, G. Kulakov, S. Maranchak, Z. Petrova, J. Nucl. Mater., 362 (2007) 356.

[4] A.M. Savchenko, A.V. Vatulin, E.M. Glagovsky, I.I. Konovalov, A.V. Morozov, A.V. Kozlov, S.A. Ershov, V.A. Mishunin, G.V. Kulakov, V.I. Sorokin, A.P. Simonov, Z.N. Petrova, V.V. Fedotov, J. Nucl. Mater., 396 (2010) 26.

[5] G. Lagerberg, J. Nucl. Mater., 9 (1963) 261.

[6] L. Leibowitz, R.A. Blomquist, A.D. Pelton, J. Nucl. Mater., 167 (1989) 76.

[7] P.Y. Chevalier, E. Fischer, J. Nucl. Mater., 257 (1998) 213.

[8] M. Kurata, T. Ogata, K. Nakamura, T. Ogawa, J. Alloys Compd., 271/273 (1998) 636.

[9] ASM Alloy Phase Diagrams Center, P. Villars, editor-in-chief; H. Okamoto, K. Cenzual, section editors; http://www1.asminternational.org/AsmEnterprise/APD, ASM International, Materials Park, OH, 2006.

[10] C.H. Thomas, E.C. Sykes, P.E. Madsen, P.C.L. Pfeil, A.E.R.E. M/R 1497, Atomic Energy Research Establishment, 1954.

[11] F.A. Rough, Report No. BMI-1030, Battelle Memorial Institute, 1955.

[12] A.A. Bauer, Report No. BMI-1350, Battelle Memorial Institute, 1959.

[13] R.F. Hills, B.R. Butcher, B.W. Howlett, D. Stewart, J. Nucl. Mater., 16 (1965) 25.

[14] C. Basak, G.J. Prasad, H.S. Kamath, N. Prabhu, J. Alloys Compd., 480 (2009) 857.

[15] C. Basak, R. Keswani, G.J. Prasad, H.S. Kamath, N. Prabhu, J. Alloys Compd., 471 (2009) 544.

[16] C. Basak, R. Keswani, G.J. Prasad, H.S. Kamath, N. Prabhu, S. Banerjee, J. Nucl. Mater., 393 (2009) 146.

[17] C. Basak, Issue No. 316, BARC Newsletter, 2010.

[18] C. Basak, J. Nucl. Mater., 416 (2011) 280.

[19] T. Ogata, M. Akabori, A. Itoh, T. Ogawa, J. Nucl. Mater., 232 (1996) 125.

[20] M. Akabori, A. Itoh, T. Ogawa, T. Ogata, J. Alloys Compd., 271-273 (1998) 597.

[21] ImageJ, W.S. Rasband; http://imagej.nih.gov/ij/, U.S. National Institutes of Health, Bethesda, MD, 1997-2012.

[22] M. Akabori, A. Itoh, T. Ogawa, F. Kobayashi, Y. Suzuki, J. Nucl. Mater., 188 (1992) 249.

[23] S.T. Zegler, Report No. ANL-6055, Argonne National Laboratory, 1962.

[24] B.D. Cullity, Elements of X-Ray Diffraction, 2nd ed., Addison-Wesley, Reading, MA, 1978.

[25] P.J. Potts, A Handbook of Silicate Rock Analysis, Chapman and Hall, New York, 1987.
[26] K. Kanaya, S. Okayama, J. Phys. D: Appl. Phys., 5 (1972) 43.
[27] P. Villars, Pearson's Handbook of Crystallographic Data for Intermetallic Phases, ASM International, Materials Park, OH, 1997.

## Tables

**Table 1.** Crystallographic data for α-U and δ-$UZr_2$ [27].

| | **Unit cell** | **Space group** | **Lattice constant (Å)** | | |
|---|---|---|---|---|---|
| | | | ***a*** | ***b*** | ***c*** |
| **α-U** | Orthorhombic | Cmcm | 2.854 | 5.870 | 4.956 |
| **δ-$UZr_2$** | Hexagonal | P6/mmm | 5.030 | 5.030 | 3.080 |

**Figures**

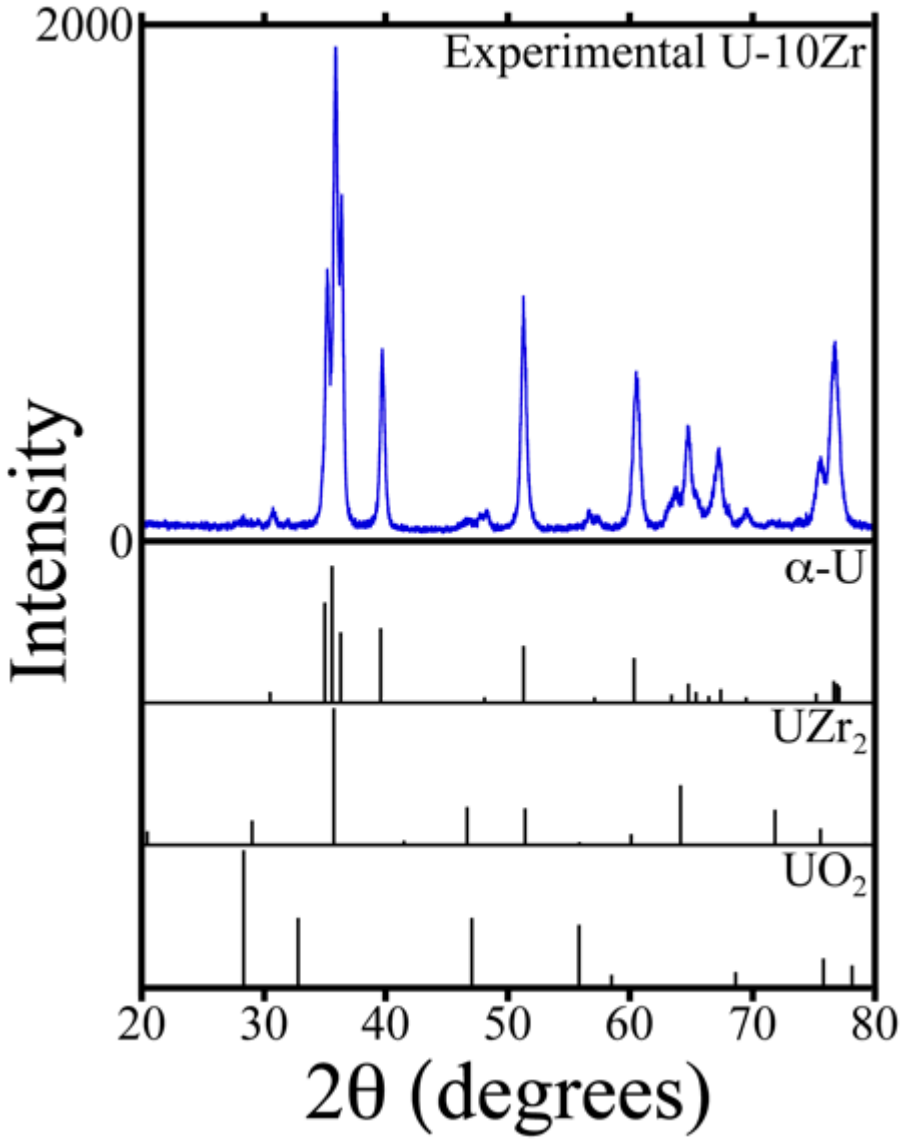


**Figure 1.** Experimental XRD data acquired from the as-cast U-10Zr alloy, with the positions of diffraction peaks for α-U, $UZr_2$, and $UO_2$ (from the powder diffraction files).

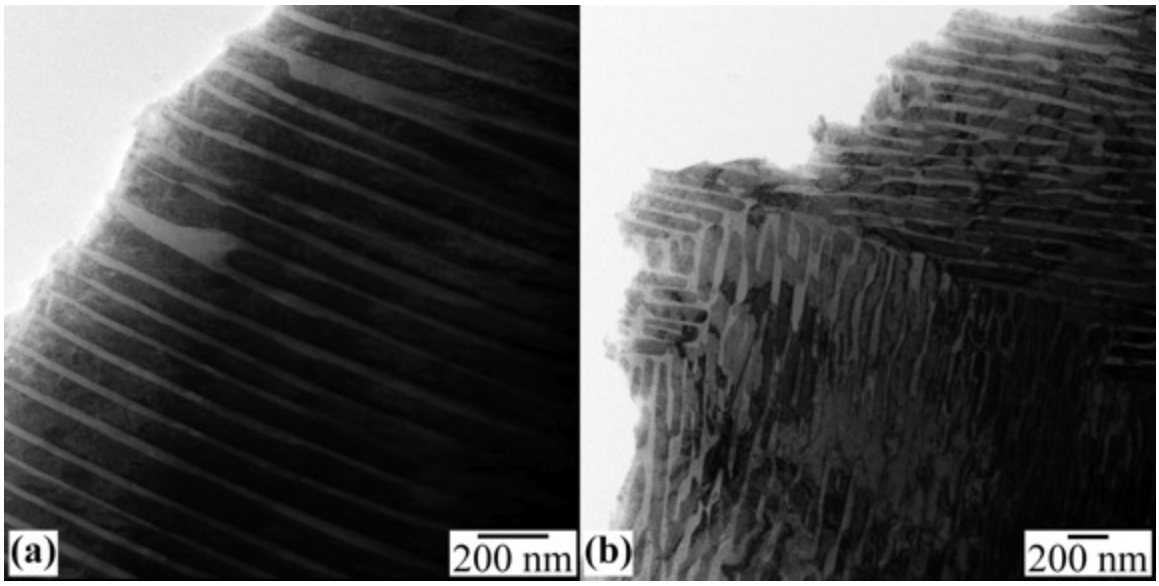


**Figure 2.** (a,b) Bright-field TEM images of the as-cast U-10Zr alloy showing alternating lamella, with adjacent variants of the lamellar structure evident in (b).

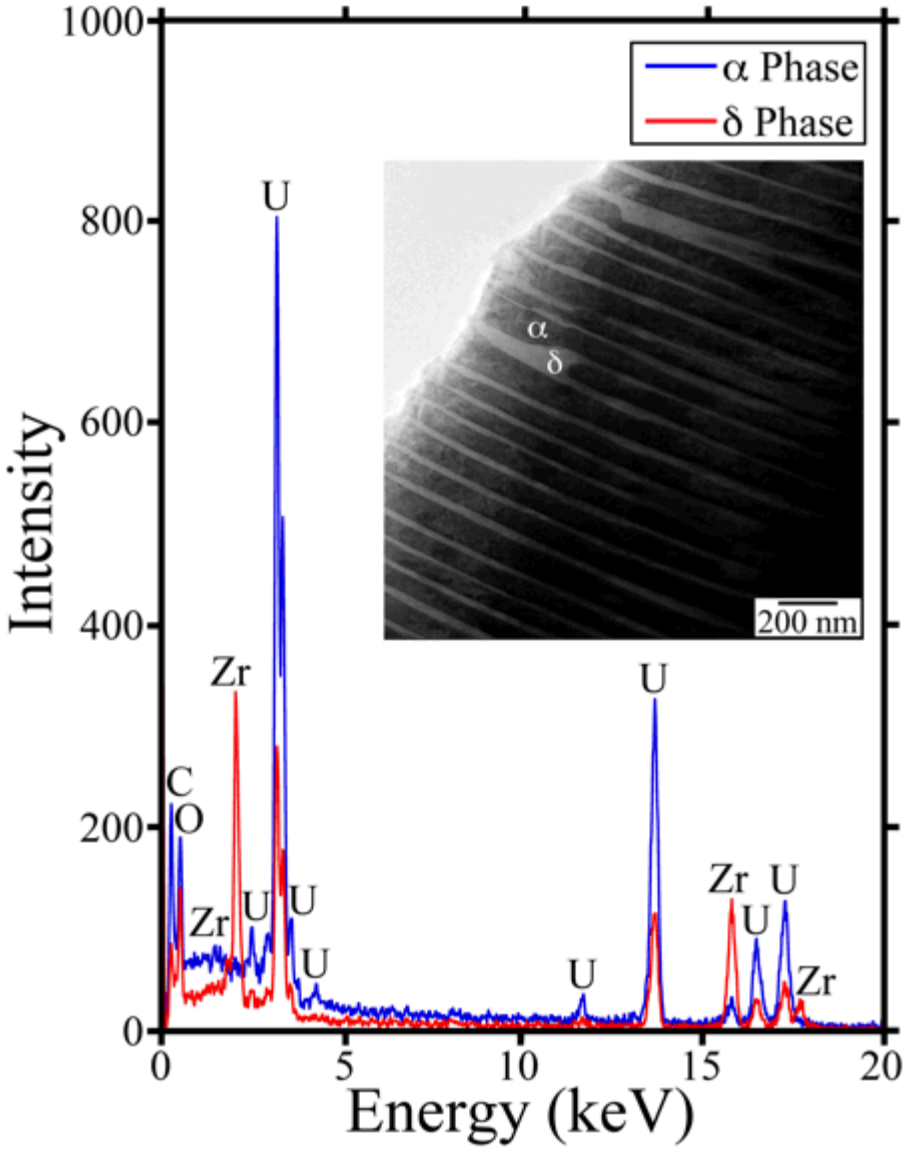


**Figure 3.** Representative EDS spectra from the alternating lamella, indicating that the lamellar structure consists of the equilibrium α (dark contrast) and δ (light contrast) phases, as labeled in the inset image.

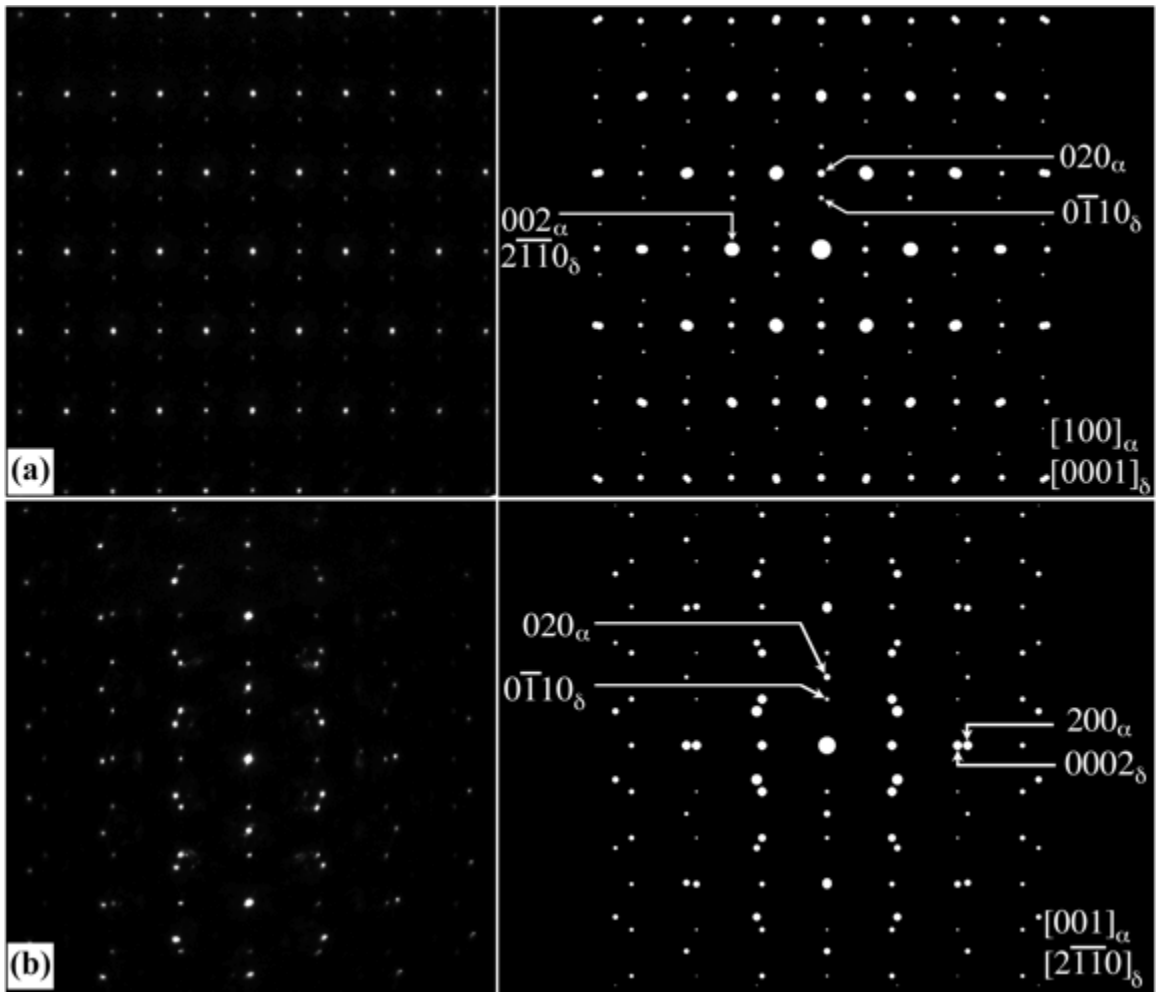


**Figure 4.** Experimental (left) and simulated (right) selected-area diffraction patterns showing the orientation relationship between the α and δ phases: (a) and (b) . These are the same orientation relationship, rotated 90° from one another about the [020] direction of the α phase. The diffraction patterns were obtained from different variants of the structure. The simulated patterns are indexed.